# Elastic Foundation Solution for the Energy Release Rate and Mode Partitioning of Face/Core Debonds in Sandwich Composites

**George A. Kardomateas**
Professor
School of Aerospace Engineering,
Georgia Institute of Technology,
Atlanta, GA 30332-0150
e-mail: george.kardomateas@aerospace.gatech.edu

**Niels Pichler**
School of Aerospace Engineering,
Georgia Institute of Technology,
Atlanta, GA 30332-0150
e-mail: niels.pichler@gmail.com

**Zhangxian Yuan**
School of Aerospace Engineering,
Georgia Institute of Technology,
Atlanta, GA 30332-0150
e-mail: yuanzx@gatech.edu

*The goal of this paper is to derive closed form expressions for the energy release rate and mode partitioning of face/core debonds in sandwich composites, which include loading in shear. This is achieved by treating a finite length sandwich beam as having a "debonded" section where the debonded top face and the substrate (core and bottom face) are free and a "joined" section where a series of springs (elastic foundation) exists between the face and the substrate. The elastic foundation analysis is comprehensive and includes the deformation of the substrate part (unlike other elastic foundation studies in the literature) and is done for a general asymmetric sandwich construction. A J-integral approach is subsequently used to derive a closed form expression for the energy release rate. In the context of this elastic foundation model, a mode partitioning approach based on the transverse and axial displacements at the beginning of the elastic foundation ("debond tip") is proposed. The results are compared with finite element results and show very good agreement.* [DOI: 10.1115/1.4044364]

*Keywords: sandwich composite, debond, interface, crack, elastic foundation*

## Introduction

A sandwich structure is a trimaterial (two stiff metallic or composite thin face sheets separated by a thick core of low density). In addition, it can be asymmetric (two faces not of the same material/thickness). A serious damage mode in these sandwich structures is the face/core debonding, which may be induced by loads encountered during service combined with environmental exposure (e.g., thermal loads, inducing decohesion primarily due to the elastic and/or thermal mismatch between the face sheet and the core) or from manufacturing imperfections. These debonds can pose a threat to the structural integrity of the component, as they can grow and completely delaminate the face sheet. To assess the criticality of face/core debonds, the associated energy release rate and the mode mixity are needed. Due to these complexities and the many possibilities of sandwich construction in terms of material choices and geometry, the energy release rate and mode mixity of a face/core debond are currently mostly determined from finite element analyses and specific to the design tests. This makes difficult and time-consuming to conduct damage tolerance and optimization design studies, especially when it comes to fatigue debond growth, in which the debond geometry is continuously changing. It also makes it very difficult to construct and promulgate specific but simple rules and tests for assuring damage tolerance. Furthermore, the fact that a sandwich is a trimaterial, rather than a bimaterial, makes it improper to directly import debond bimaterial relations, which may exist in the literature. Another issue unique to sandwich is the very large transverse shear due to the weak core and its effect to debond growth, which makes the mixed-mode face/core sandwich debond problem a unique research item.

Regarding closed form solutions, the trimaterial crack problem without transverse shear was solved by Kardomateas et al. [1] and Østergaard and Sørensen [2]. Previously, the bimaterial crack problem, again without shear, had been solved by Suo and Hutchinson [3]. Then, researchers further extended the approach in Ref. [2] to include the shear effect. Li et al. [4] studied the shear effect on the bimaterial crack problem by a semi-numerical approach (finite elements used to determine quantities that enter into direct expressions). Similar semi-numerical approaches were used by Andrews and Massabò [5] to study the energy release rate and mode mixity of a crack in a homogeneous solid, and more recently, the same semi-numerical approach was used by Barbieri et al. [6] to study a sandwich specimen with symmetric face sheets subjected to shear loading. Note that we use the expression "semi-numerical" in the same context as the word "semi-analytical" used in Ref. [6], i.e., to refer to an approach in which some coefficients appearing in the formulation require to be determined via a numerical (most commonly finite element) approach. Although the approach presented in this paper is a fully closed form approach, it employs a beam theory and, thus, it is expected to suffer from the approximations of beam theory assumptions, unlike the aforementioned semi-analytic/semi-numerical approaches.

In the closed form approach of Refs. [1,2], the J-integral was used to derive the energy release rate and the complex stress intensity factor method was used to decompose the modes. These approaches are, however, not suitable when shear is present, because in this case, the displacement slopes enter into the J-integral expression, and the J-integral cannot be expressed as the squared norm of a single complex number. The limitations of treatments of Refs. [1,2] regarding their applicability to fracture mechanics specimens are extensively discussed in Ref. [6].

One of the approaches that could be used to analyze a face/core debond, and include the effect of shear, is the elastic foundation (EF) approach. In this approach, the top debonded face is considered to rest on an elastic foundation, which is provided by the rest of the structure, i.e., the core and the bottom face. Such elastic foundation

Contributed by the Applied Mechanics Division of ASME for publication in the Journal of Applied Mechanics. Manuscript received March 8, 2019; final manuscript received July 24, 2019; published online July 26, 2019. Assoc. Editor: Shengping Shen.

  

models have been used from the 1970s for the study of crack propagation. Kanninen [7] used such a model for the study of the double cantilever beam (DCB) test specimen in a homogeneous material with the crack at mid-thickness. Williams [8] extended Kanninen's model using the Timoshenko beam theory in a homogeneous material, and he used a formula for the elastic foundation constant similar to Kanninen's [7] based on the thickness of the debonded layer. More recently, Thouless [9] demonstrated that Kanninen's solution can be explained using the models in Refs. [4,5].

In a recent study, Li and Carlsson [10] analyzed the tilted sandwich debond specimen using an elastic foundation approach with a Kanninen-type formula for the foundation modulus. Even more recently, Saseendran et al. [11] presented an elastic foundation analysis of moment- and force-loaded single cantilever beam sandwich fracture specimens in conjunction with finite element analysis (FEA). In these studies, either the crack was in the middle of the thickness in a homogeneous solid [7,8] or the substrate was assumed rigid, i.e., only the face sheet was analyzed [10,11]. With these assumptions, the effects of the end fixity at the bonded segment was not included. Also, a closed form mode mixity derivation was not attempted in these studies.

In these elastic foundation analyses, a key question concerns the proper formula for the elastic foundation modulus. In this regard, Kardomateas et al. [12] conducted a comprehensive study that resulted in a closed form expression for both the normal and shear spring stiffnesses. The formulas were derived based on both the elasticity solution (as a benchmark) and the extended high-order sandwich panel theory [13], which is the most accurate sandwich structural theory to date. Simple approximate formulas of high accuracy, updating the ones by Kanninen [7], were also suggested.

In this paper, we present a complete closed form solution for the energy release rate and mode partitioning of a face/core debond, which includes both the face and the substrate as well as the end fixity (e.g., simply supported or clamped). The mode partitioning proposed in the context of this elastic foundation model is based on the displacement field. The Euler–Bernoulli theory (with a shear correction angle) is utilized to analyze both the debonded part and the substrate parts. Notice that the shear correction angle is an approximate way to account for shear, which is neglected in the formulation of the Euler–Bernoulli theory. The alternative would be the Timoshenko beam theory, which is a beam theory with an extra generalized coordinate (the shear deformation), but this approach would result in far more involved relations. In fact, the Euler–Bernoulli theory is used to derive the displacement field and the shear correction angle is employed later in the formulation of the J-integral (as in Refs. [5,6]) and the definition of the mode partitioning measure. Results are presented and compared with data from corresponding finite element analyses. It should also be noted at this point that the Euler–Bernoulli theory with a shear correction angle has been used in the literature to derive simple closed form solutions for many problems, see, for example, the Engesser-type formula for column buckling in the Timoshenko and Gere book [14]. It is a very efficient way to account for transverse shear and, yet, take advantage of the simplicity of the Euler–Bernoulli beam theory. The elastic foundation approach based on the Timoshenko beam theory for both the debonded and the substrate parts is the next step in our research and will be the topic of a separate paper.

## Formulation

We consider a sandwich beam of width $b$ consisting of a top and a bottom face sheet of thickness $f_t$ and $f_b$, extensional Young's modulus (along $x$) $E_{ft}$ and $E_{fb}$, respectively (assumed to be equal in tension and compression), and a core of thickness $2c$, with an extensional Young's modulus (along $x$), $E_c$, again assumed to be equal in tension and compression (Fig. 1(*a*)). Note that since only Young's modulus along the axial direction appears in the Euler–Bernoulli formulation, both faces and core can be either isotropic or orthotropic.

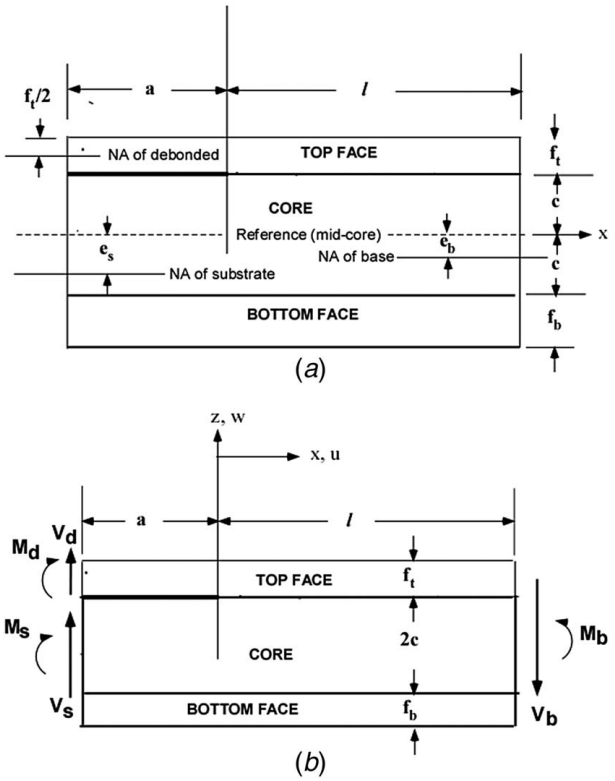


**Fig. 1 (*a*) The debonded sandwich geometry definitions and (*b*) loads and coordinate system definitions**

Over the region of the debond, the sandwich beam consists of two parts: the debonded upper face sheet (referred to as the "debonded part" of thickness $f_t$) and the part below the debond ("substrate part" of thickness $2c+f_b$, which includes the core and the lower face sheet). We shall denote the debonded part with "d" and the substrate part with "s."

A characteristic of a sandwich beam with a debond is that while for the debonded face, which is homogeneous, the neutral axis is at mid-thickness, for the substrate part, the neutral axes is no longer at the geometrical mid-point of the section. With respect to a reference axis $x$ through the middle of the core, the neutral axis of the substrate part is at a distance $e_s$

$$e_s\left[E_c(2c)+E_{ft}f_b\right]=E_{ft}f_b\left(\frac{f_b}{2}+c\right) \tag{1a}$$

Moreover, while for the debonded face sheet, which is homogeneous, the bending rigidity is

$$(EI)_d=E_{ft}\frac{bf_t^3}{12} \tag{1b}$$

for the substrate, the flexural rigidity is

$$(EI)_s = b\left[E_c\frac{2c^3}{3}+E_c(2c)e_s^2+E_{fb}\frac{f_b^3}{12}+E_{ft}f_b\left(\frac{f_b}{2}+c-e_s\right)^2\right] \tag{1c}$$

It should be noted that the formulation and approach are applicable to both beams (plane stress) and wide panels (plane strain) but different moduli should be used for plane strain and plane stress problems. For plane stress, Eq. (1*c*), with $E$ being Young's modulus, is applicable. For plane strain, $E$ in Eq. (1*c*) should be replaced by $E/(1-\nu^2)$, where $\nu$ is Poisson's ratio.

However, the J-integral formula is somewhat different for beams (plane stress) and wide panels (plane strain) and this is explained in

the J-integral section. In fact, whenever differences exist between plane stress and plane strain in the formulas presented in the following, it will be pointed out.

Figure 1(*b*) shows a segment of the beam containing the debond configuration, where a debond of length $a$ and an intact part of length $l$ exist. Notice that in this paper, we focus on the overall behavior of a sandwich beam with an interfacial debond; thus, the debond length can be arbitrary.

The debonded part is loaded by a shear force $V_d$ and a moment $M_d$, the substrate part is loaded by a shear force $V_s$ and a moment $M_s$, and at the end, a shear force $V_b$ and a moment $M_b$ exist. Equilibrium of these forces and moments yields

$$V_b = V_d + V_s; \quad M_b = M_d + M_s + (V_d + V_s)(l + a) \tag{1d}$$

The coordinate system is set so that $x = 0$ is at the end of the debond, i.e., the debond is for negative $x$ and the intact part is for positive $x$. We denote by $w$ and $u$ the transverse and axial displacements, respectively.

The elastic foundation load is a distributed load applied to both the debonded part and the substrate. Thus, the governing equations are

$$(EI)_d \frac{d^4 w_d}{dx^4} + S(x) k_n (w_d - w_s) = 0 \tag{2a}$$

$$(EI)_s \frac{d^4 w_s}{dx^4} + S(x) k_n (w_s - w_d) = 0 \tag{2b}$$

where $k_n$ is the modulus of the elastic foundation. Notice that the governing equations (2*a*) and (2*b*) are based on the Euler–Bernoulli theory, and shear deformation is not accounted for at this stage.

The function $S(x)$ is a step function allowing to separate the portion of the beam where they are linked, $x > 0$, and where they are not, $x < 0$, i.e.,

$$S(x) = \begin{cases} 1 & \text{if } x > 0 \\ 0 & \text{if } x < 0 \end{cases} \tag{2c}$$

For the joined part $0 \le x \le l$, in which case $S(x) = 1$, substituting $w_d$ from (2*b*) into (2*a*) results in

$$\frac{(EI)_s}{k_n} \frac{d^8 w_s}{dx^8} + \left[1 + \frac{(EI)_s}{(EI)_d}\right] \frac{d^4 w_s}{dx^4} = 0 \tag{2d}$$

with

$$w_d = \frac{(EI)_s}{k_n} \frac{d^4 w_s}{dx^4} + w_s \tag{2e}$$

Setting

$$\lambda^4 = k_n \frac{(EI)_d + (EI)_s}{4(EI)_d (EI)_s} \tag{3a}$$

Equation (2*d*) can be written in the form

$$\frac{d^8 w_s}{dx^8} + 4\lambda^4 \frac{d^4 w_s}{dx^4} = 0 \tag{3b}$$

A comprehensive study on the proper value of the elastic foundation modulus was conducted by Kardomateas et al. [12] by deriving the value from elasticity theory and the extended high-order sandwich panel theory [13]. This study showed that a very good approximation of the elastic foundation modulus is given by

$$k_n = \frac{c_{33}^c}{c} b \tag{3c}$$

where

$$c_{33}^c = E_3^c \frac{\left(1 - \nu_{12}^c \nu_{21}^c\right)}{1 - \left(\nu_{12}^c \nu_{21}^c + \nu_{23}^c \nu_{32}^c + \nu_{13}^c \nu_{31}^c\right) - \left(\nu_{12}^c \nu_{23}^c \nu_{31}^c + \nu_{21}^c \nu_{32}^c \nu_{13}^c\right)} \tag{3d}$$

where we have adopted the convention $1 \equiv x$, $2 \equiv y$, and $3 \equiv z$; $E_3^c$ is the transverse extensional modulus of the core; and the $\nu$'s are Poisson's ratios of the core.

The solution to Eq. (3*b*) consists of a trigonometric/hyperbolic part $H(x)$ and a polynomial part $P(x)$

$$w_s = H(x) + P(x) \tag{4a}$$

where

$$\begin{aligned} H(x) = {} & C_1 \cosh \lambda x \cos \lambda x + C_2 \cosh \lambda x \sin \lambda x \\ & + C_3 \sinh \lambda x \cos \lambda x + C_4 \sinh \lambda x \sin \lambda x \end{aligned} \tag{4b}$$

and

$$P(x) = C_5 x^3 + C_6 x^2 + C_7 x + C_8 \tag{4c}$$

Notice that function $H(x)$ has the property

$$\frac{d^4 H(x)}{dx^4} = -4\lambda^4 H(x) \tag{4d}$$

Thus, from (2*e*)

$$w_d = H(x)\left[1 - 4\lambda^4 \frac{(EI)_s}{k_n}\right] + P(x) \tag{4e}$$

$$w_d = \beta H(x) + P(x) \tag{4f}$$

where from (3*a*)

$$\beta = 1 - 4\lambda^4 \frac{(EI)_s}{k_n} = -\frac{(EI)_s}{(EI)_d} \tag{4g}$$

For the debonded part $-a \le x \le 0$, for which $S(x) = 0$, the solution is simply a third-order polynomial

$$w_d = A_d x^3 + B_d x^2 + C_d x + D_d \tag{5a}$$

$$w_s = A_s x^3 + B_s x^2 + C_s x + D_s \tag{5b}$$

At the end, $x = l$, the total shear is the sum of the shear created by the debonded and substrate parts, i.e.,

$$\begin{aligned} V_b &= (EI)_d \left.\frac{d^3 w_d}{dx^3}\right|_{x=l} + (EI)_s \left.\frac{d^3 w_s}{dx^3}\right|_{x=l} \\ &= (EI)_d \beta \left.\frac{d^3 H}{dx^3}\right|_{x=l} + (EI)_d 6C_5 + (EI)_s \left[\left.\frac{d^3 H}{dx^3}\right|_{x=l} + 6C_5\right] \end{aligned} \tag{6a}$$

where we have used (4*a*), (4*c*), and (4*f*).

Substituting $\beta = -(EI)_s/(EI)_d$ from (4*g*), Eq. (6*a*) results in

$$6C_5 = \frac{V_b}{(EI)_d + (EI)_s} \tag{6b}$$

Similarly, at the end, $x = l$, the total moment is the sum of the

moments created by the debonded and substrate parts, i.e.,

$$M_b = (EI)_d \left.\frac{d^2 w_d}{dx^2}\right|_{x=l} + (EI)_s \left.\frac{d^2 w_s}{dx^2}\right|_{x=l}$$
$$= (EI)_d \beta \left.\frac{d^2 H}{dx^2}\right|_{x=l} + (EI)_d (6C_5 l + 2C_6) \tag{7a}$$
$$+ (EI)_s \left[\left.\frac{d^2 H}{dx^2}\right|_{x=l} + (6C_5 l + 2C_6)\right]$$

Again, substituting $\beta = -(EI)_s/(EI)_d$ from (4g), Eq. (7a) results in

$$6C_5 l + 2C_6 = \frac{M_b}{(EI)_d + (EI)_s} \tag{7b}$$

which using (6b) results in

$$2C_6 = \frac{M_b - V_b l}{(EI)_d + (EI)_s} \tag{7c}$$

Thus, two of the constants in the polynomial $P(x)$ have been obtained in (6b) and (7c).

The remaining two constants of the polynomial, the $C_7$ and $C_8$, will be found later from the conditions at the end. Notice that this residual part of the polynomial $P(x)$, the $C_7 x + C_8$, produces no strain (since the strain in the Euler–Bernoulli theory is associated with the bending moment and shearing force, which in turn are expressed in terms of the second and third derivatives of the displacement).

At the debond tip section, $x = 0$, we have continuity conditions for $w_s|_{x=0}$ and the derivatives up to third order, with the function defined in (4a) for $x \geq 0$ and in (5b) for $x \leq 0$; same for $w_d|_{x=0}$ defined in (4f) for $x \geq 0$ and in (5a) for $x \leq 0$, which gives

$$\text{function: } D_d = \beta H(0); \quad D_s = H(0) \tag{8a}$$

$$\text{First derivative: } C_d = \beta H_{,x}(0); \quad C_s = H_{,x}(0) \tag{8b}$$

$$\text{Second derivative: } 2B_d = \beta H_{,xx}(0) + 2C_6; \quad 2B_s = H_{,xx}(0) + 2C_6 \tag{8c}$$

$$\text{Third derivative: } 6A_d = \beta H_{,xxx}(0) + 6C_5; \quad 6A_s = H_{,xxx}(0) + 6C_5 \tag{8d}$$

At the loaded left end, $x = -a$, we apply (5a) and (5b) to obtain the following equations that determine $A_d$, $A_s$, $B_d$, and $B_s$:

$$V_d = (EI)_d \left.\frac{d^3 w_d}{dx^3}\right|_{x=-a} \quad \text{or} \quad 6A_d = \frac{V_d}{(EI)_d} \tag{9a}$$

$$V_s = (EI)_s \left.\frac{d^3 w_s}{dx^3}\right|_{x=-a} \quad \text{or} \quad 6A_s = \frac{V_s}{(EI)_s} \tag{9b}$$

$$M_d = (EI)_d \left.\frac{d^2 w_d}{dx^2}\right|_{x=-a} \quad \text{or} \quad -6A_d a + 2B_d = \frac{M_d}{(EI)_d} \tag{9c}$$

$$M_s = (EI)_s \left.\frac{d^2 w_s}{dx^2}\right|_{x=-a} \quad \text{or} \quad -6A_s a + 2B_s = \frac{M_s}{(EI)_s} \tag{9d}$$

From (9a) and (8d), we obtain

$$6C_5 = 6A_d - \beta H_{,xxx}(0) = \frac{V_d}{(EI)_d} - \beta H_{,xxx}(0) \tag{10a}$$

Similarly, from (9b) and (8d), we obtain

$$6C_5 = 6A_s - H_{,xxx}(0) = \frac{V_s}{(EI)_s} - H_{,xxx}(0) \tag{10b}$$

Although it may look at this point that we have more equations than unknowns, this is not true, because of the equilibrium conditions. In fact, multiplying (10b) by $-\beta$ and adding to (10a) and using (4g) gives

$$6C_5 = \frac{V_d + V_s}{(EI)_d + (EI)_s} = \frac{V_b}{(EI)_d + (EI)_s} \tag{11}$$

which is the same as Eq. (6b) since $V_b = V_d + V_s$ from the equilibrium (1d).

Similarly, from (10b), (9d), and (8c), we obtain

$$2C_6 = \frac{M_s}{(EI)_s} + \frac{V_s}{(EI)_s} a - H_{,xx}(0) \tag{12a}$$

and from (10a), (9c), and (8c)

$$2C_6 = \frac{M_d}{(EI)_d} + \frac{V_d}{(EI)_d} a - \beta H_{,xx}(0) \tag{12b}$$

Multiplying (12a) by $-\beta$, adding (12b), and considering (4g) results in

$$2C_6 = \frac{M_d + M_s + (V_d + V_s)a}{(EI)_d + (EI)_s} \tag{12c}$$

Substituting $M_d + M_s$ and $V_d + V_s$ from equilibrium (1d) gives

$$2C_6 = \frac{M_b - V_b l}{(EI)_d + (EI)_s} \tag{12d}$$

which is the same as (7c).

Until now, we have mostly defined the coefficients of the polynomial $P(x)$ (Eq. (4c)), so next we will formulate the system for the coefficients of $H(x)$ (Eq. (4b)). Substituting $\beta = -(EI)_s/(EI)_d$ in (10a) and (10b)

$$2H_{,xxx}(0) = \frac{V_s - V_d}{(EI)_s} + 6C_5 \left[\frac{(EI)_d}{(EI)_s} - 1\right] \tag{13a}$$

Using (11) for $C_5$ leads to

$$H_{,xxx}(0) = \frac{1}{2(EI)_s} \left\{V_s - V_d + V_b \left[\frac{(EI)_d - (EI)_s}{(EI)_d + (EI)_s}\right]\right\} \tag{13b}$$

or

$$2\lambda^3 (C_2 - C_3) = \frac{1}{2(EI)_s} \left\{V_s - V_d + V_b \left[\frac{(EI)_d - (EI)_s}{(EI)_d + (EI)_s}\right]\right\} \tag{13c}$$

Similarly, from (12a) and (12b), we obtain

$$2H_{,xx}(0) = \frac{M_s - M_d}{(EI)_s} + \frac{V_s - V_d}{(EI)_s} a + 6C_6 \left[\frac{(EI)_d}{(EI)_s} - 1\right] \tag{14a}$$

Using (12d) for $C_6$ leads to

$$H_{,xx}(0) = \frac{1}{2(EI)_s} \left\{M_s - M_d + (V_s - V_d)a + (M_b - V_b l)\left[\frac{(EI)_d - (EI)_s}{(EI)_d + (EI)_s}\right]\right\} \tag{14b}$$

or

$$2\lambda^2 C_4 = \frac{1}{2(EI)_s} \left\{M_s - M_d + (V_s - V_d)a + (M_b - V_b l)\left[\frac{(EI)_d - (EI)_s}{(EI)_d + (EI)_s}\right]\right\} \tag{14c}$$

Next, we impose continuity of displacement and slope of the two domains at $x = 0$.

By using (4*a*) and (5*b*) for the definitions of $w_s$ in the two domains ($x \geq 0$ and $x \leq 0$, respectively), we obtain

$$H(0) = D_s \quad \text{or} \quad C_1 = D_s \tag{15a}$$

$$H_{,x}(0) = C_s \quad \text{or} \quad \lambda(C_2 + C_3) = C_s \tag{15b}$$

Similarly, using (4*f*) and (5*a*) for the definitions of $w_d$ in the two domains ($x \geq 0$ and $x \leq 0$, respectively), we obtain

$$\beta H(0) = D_d \quad \text{or} \quad \beta C_1 = D_d \tag{15c}$$

and

$$\beta H_{,x}(0) = C_d \quad \text{or} \quad \beta\lambda(C_2 + C_3) = C_d \tag{15d}$$

The conditions at $x = l$ depend on the end fixity of the structure. We shall formulate the case of a clamped end in this paper, so at $x = l$, we impose the condition of same displacement and slope of the debonded and substrate parts, in which case, the condition

$$w_s(l) = w_d(l) \tag{16a}$$

leads from (4*a*) and (4*f*) to

$$H(l) = 0 \tag{16b}$$

which, from (4*b*), becomes

$$C_1 \cosh \lambda l \cos \lambda l + C_2 \cosh \lambda l \sin \lambda l + C_3 \sinh \lambda l \cos \lambda l + C_4 \sinh \lambda l \sin \lambda l = 0 \tag{16c}$$

At this point, it is important to note that the hyperbolic cos and sin functions can quickly become very large numbers, unlike the hyperbolic tan function, and this would make the numerical solution fail, thus we divide by cosh $\lambda l$, to obtain

$$C_1 \cos \lambda l + C_2 \sin \lambda l + C_3 \tanh \lambda l \cos \lambda l + C_4 \tanh \lambda l \sin \lambda l = 0 \tag{16d}$$

The condition

$$w_{s,x}(l) = w_{d,x}(l) \tag{16e}$$

leads from (4*a*) and (4*f*) to

$$H_{,x}(l) = 0 \tag{16f}$$

which, from (4*b*), becomes

$$C_1(\sinh \lambda l \cos \lambda l - \cosh \lambda l \sin \lambda l) + C_2(\sinh \lambda l \sin \lambda l + \cosh \lambda l \cos \lambda l) + C_3(\cosh \lambda l \cos \lambda l - \sinh \lambda l \sin \lambda l) + C_4(\cosh \lambda l \sin \lambda l + \sinh \lambda l \cos \lambda l) = 0 \tag{16g}$$

Similarly, to avoid numerical failure, we divide by cosh $\lambda l$ to obtain

$$C_1(\tanh \lambda l \cos \lambda l - \sin \lambda l) + C_2(\tanh \lambda l \sin \lambda l + \cos \lambda l) + C_3(\cos \lambda l - \tanh \lambda l \sin \lambda l) + C_4(\sin \lambda l + \tanh \lambda l \cos \lambda l) = 0 \tag{16h}$$

Equations (13*c*), (14*c*), (16*d*), and (16*h*) can be solved for $C_1$, $C_2$, $C_3$, and $C_4$. Thus, Eqs. (13*a*)–(14*c*) and (16*a*)–(16*h*) determine the unknown constants in $H(x)$. Also, notice that Eqs. (8*a*)–(8*d*) and (15*a*)–(15*d*) determine the constants in $w_d$ and $w_s$ (Eqs. (5*a*) and (5*b*)).

Let us set

$$V_0 = V_s - V_d + V_b\left[\frac{(EI)_d - (EI)_s}{(EI)_d + (EI)_s}\right] \tag{17a}$$

$$M_0 = M_s - M_d + (V_s - V_d)a + (M_b - V_b l)\left[\frac{(EI)_d - (EI)_s}{(EI)_d + (EI)_s}\right] \tag{17b}$$

Then, in terms of

$$b_1 = -\frac{V_0}{4\lambda^3(EI)_s}\sin \lambda l - \frac{M_0}{4\lambda^2(EI)_s}\tanh \lambda l \sin \lambda l \tag{17c}$$

$$b_2 = -\frac{V_0}{4\lambda^3(EI)_s}(\tanh \lambda l \sin \lambda l + \cos \lambda l) - \frac{M_0}{4\lambda^2(EI)_s}(\sin \lambda l + \tanh \lambda l \cos \lambda l) \tag{17d}$$

the $C$'s in the $H(x)$ are

$$C_1 = \frac{2b_1 \cos \lambda l - b_2(\sin \lambda l + \tanh \lambda l \cos \lambda l)}{1 + \cos^2 \lambda l(1 - \tanh^2 \lambda l)} \tag{18a}$$

$$C_3 = \frac{b_2 \cos \lambda l - b_1(\tanh \lambda l \cos \lambda l - \sin \lambda l)}{1 + \cos^2 \lambda l(1 - \tanh^2 \lambda l)} \tag{18b}$$

$$C_2 = \frac{V_0}{4\lambda^3(EI)_s} + C_3 \tag{18c}$$

$$C_4 = \frac{M_0}{4\lambda^2(EI)_s} \tag{18d}$$

The other constants in the $H(x)$ are given in (11) and (12*c*).

Regarding the displacement field of the debond and substrate constants, Eq. (5), these are

From (8*a*)

$$D_s = C_1; \quad D_d = \beta C_1 \tag{19a}$$

from (8*b*)

$$C_s = \lambda(C_2 + C_3); \quad C_d = \beta\lambda(C_2 + C_3) \tag{19b}$$

from (10*a*) and (10*b*)

$$A_s = \frac{V_s}{6(EI)_s}; \quad A_d = \frac{V_d}{6(EI)_d} \tag{19c}$$

and from (8*c*), (12*a*), and (12*b*)

$$B_s = \frac{M_s + V_s a}{2(EI)_s}; \quad B_d = \frac{M_d + V_d a}{2(EI)_d} \tag{19d}$$

Finally, the remaining constants $C_7$ and $C_8$ in the polynomial $P(x)$ are determined from the boundary condition at the end, $x = l$. Assuming a clamped end would require

$$w_d(l) = w_s(l) = 0; \quad w_{d,x}(l) = w_{s,x}(l) = 0 \tag{20a}$$

From (4*a*), (4*g*), (16*b*), and (16*f*), these conditions become

$$C_5 l^3 + C_6 l^2 + C_7 l + C_8 = 0; \quad 3C_5 l^2 + 2C_6 l + C_7 = 0 \tag{20b}$$

Substituting (6*b*) and (7*c*) for $C_5$ and $C_6$ gives

$$C_7 = -\frac{M_b l}{(EI)_d + (EI)_s} + \frac{V_b l^2}{2[(EI)_d + (EI)_s]} \tag{20c}$$

$$C_8 = \frac{M_b l^2}{2[(EI)_d + (EI)_s]} - \frac{V_b l^3}{6[(EI)_d + (EI)_s]} \tag{20d}$$

Notice that different end conditions at $x = l$ would lead to a different solution. For example, a simply supported end at $x = l$ would require zero displacement and moment at $x = l$.

## J-Integral

The J-integral is defined by

$$J = \int_{\Gamma} W dz - T_i \frac{\partial u_i}{\partial x} ds \tag{21a}$$

where $W = \int_0^{\epsilon} \sigma_{ij} d\epsilon_{ij}$ is the strain energy density, and $T_i$ and $u_i$ are the components of the traction vector and the displacement vector, respectively. We will choose the integration path $\Gamma = BAA'FED'DCB$, as in Fig. 2, that follows the outer boundary of the structure.

It should be mentioned that the J-integral had already been applied in Refs. [5,6] for the purpose of obtaining the energy release rate, and we follow a similar approach in this paper by directly applying our derived displacement field in the J-integral formula in order to obtain a closed form expression for the energy release rate.

On the horizontal segments of the path, $\vec{T} = 0$ and $dz = 0$, so $J = 0$. We thus only have paths $BA$, $A'F$, $ED'$, and $D'C$ that contribute to J. Note that $ds$ becomes $dz$ or $-dz$ on these vertical paths.

On the vertical sides

$$W = \frac{1}{2}\left(\sigma_{xx}\epsilon_{xx} + \sigma_{zz}\epsilon_{zz} + \tau_{xz}\gamma_{xz}\right);$$
$$T_i \frac{\partial u_i}{\partial x} = -\sigma_{xx}\epsilon_{xx} - \tau_{xz} w_{,x} \tag{21b}$$

We assume that the shear load creates a shear stress $\tau_{xz}$ and a shear strain $\gamma_{xz} = \kappa\tau_{xz}/G_{eq}$, where $G_{eq}$ is the equivalent shear modulus of the section and $\kappa$ is the shear correction factor, which takes into account the nonuniform distribution of shear stresses due to the sandwich construction throughout the entire cross section.

The equivalent shear modulus for the section should be derived by assuming that the constituent sections are "springs in parallel," as was shown in Ref. [15]. For the debonded part, which is homogeneous, the equivalent shear modulus is

$$G_d = G_{ft} \tag{22a}$$

For the substrate part which consists of the core and the bottom face

$$\frac{2c + f_b}{G_s} = \frac{2c}{G_c} + \frac{f_b}{G_{fb}} \tag{22b}$$

Regarding the shear correction factor, for a homogeneous section, $\kappa = 6/5$. Thus, for the debonded part

$$\kappa_d = \frac{6}{5} \tag{22c}$$

For a general asymmetric sandwich section, the shear correction factor was derived in Ref. [16] from energy considerations. This formula was proven to be very effective in accounting for transverse shear in a related buckling study [17]. For a symmetric sandwich section, a simpler shear correction factor formula can be found in Ref. [17]. However, notice that the substrate part is an asymmetric sandwich section. For the substrate part, which consists only of the core and the bottom face, the general asymmetric section formula in Ref. [16] becomes

$$\kappa_s = \frac{G_s b^2 (2c + f_b)}{4(EI)_s^2}\left(\frac{E_c^2}{G_c} q_2 - \frac{E_{fb}^2}{G_{fb}} q_1\right) \tag{22d}$$

where

$$q_1 = f_b(c - e_s + f_b)^4 + \frac{1}{5}\left[(c - e_s + f_b)^5 - (c - e_s)^5\right] - \frac{2}{3}(c - e_s + f_b)^2\left[(c - e_s + f_b)^3 - (c - e_s)^3\right] \tag{22e}$$

and

$$q_2 = 2c(c + e_s)^4 + \frac{1}{5}\left[(c + e_s)^5 + (c - e_s)^5\right] - \frac{2}{3}(c + e_s)^2\left[(c + e_s)^3 + (c - e_s)^3\right] \tag{22f}$$

Now, returning to the J-integral, Eq. (21a), we note that on the vertical sides of the J-integral path

$$\sigma_{xx} = E_i \frac{M_i s}{(EI)_{eq}}; \quad \tau_{xz} = \frac{-V_i}{A}; \quad i = d, s, b \tag{23a}$$

where $E_i$ refers to the point in question, i.e., $E_i = E_c$ if it is in the core, $E_i = E_{ft}$ if in the top face, etc. Also, $(EI)_{eq}$ is the equivalent bending rigidity of the section, for example, for the substrate part, $(EI)_{eq} = (EI)_s$, for the base part, $(EI)_{eq} = (EI)_b$, etc.

Thus, on the BA segment (top face-left side), on which $dz = -ds$ (Fig. 3)

$$dJ = \left[\frac{1}{2}\left(\sigma_{xx}\epsilon_{xx} - \sigma_{zz}\epsilon_{zz} - \tau_{xz}\gamma_{xz}\right) + \tau_{xz} w_{,x}\right] ds \tag{23b}$$

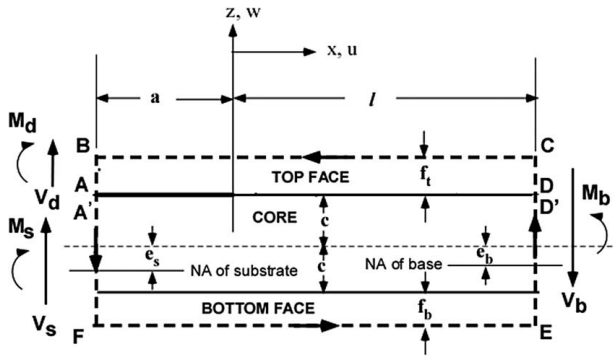


**Fig. 2 J-integral path**

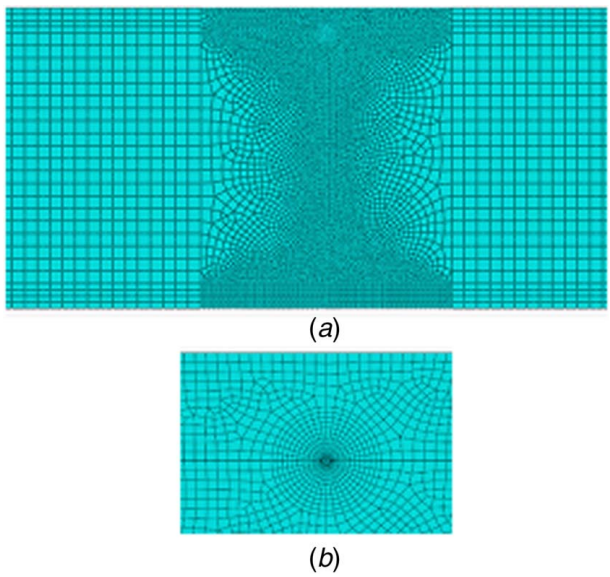


**Fig. 3 Finite element mesh: (*a*) mesh at the region near the crack tip and (*b*) detail of the crack tip mesh**

From a plane stress assumption, $\sigma_{zz}=0$, and $\epsilon_{xx}=\sigma_{xx}/E$, thus

$$dJ=\left[\frac{1}{2E}\sigma_{xx}^2-\frac{\kappa}{2G_{eq}}\tau_{xz}^2+\tau_{xz}w_{,x}\right]ds \tag{23c}$$

Notice that for a plane strain assumption, $\epsilon_{zz}=0$, we would have $\sigma_{zz}=\nu_{xz}\sigma_{xx}$, therefore, $\epsilon_{xx}=(\sigma_{xx}-\nu_{zx}\sigma_{zz})/E=(1-\nu_{zx}\nu_{xz})\sigma_{xx}/E$, and the first term in (23c) should be multiplied by $(1-\nu_{zx}\nu_{xz})$.

Therefore, again for a plane stress assumption

$$\begin{aligned}J_{BA}&=\int_{-f_t/2}^{f_t/2}\left\{\frac{1}{2}\left[E_{ft}\frac{M_d^2s^2}{(EI)_d^2}-\frac{\kappa_dV_d^2}{G_dA_d^2}\right]-\frac{V_d}{A_d}\frac{dw_d}{dx}\bigg|_{x=-a}\right\}ds\\&=\frac{1}{2b^2}\left[\frac{12M_d^2}{E_{ft}f_t^3}-\frac{\kappa_dV_d^2}{G_df_t}-2V_db\ w_{d,x}(-a)\right]\end{aligned} \tag{24}$$

The only dependence of $J_{BA}$ on the displacements is the $dw_d/dx$ at $x=-a$, which is the rotation of the beam at its end. For every part of the path, $w_i$ will only appear as a first order derivative evaluated at a boundary.

Similarly, for $J_{A'F}$ (substrate part-left side)

$$\begin{aligned}J_{A'F}&=\int_{A'F}\left\{\frac{1}{2}\left[E_i\frac{M_s^2s^2}{(EI)_s^2}-\frac{\kappa_sV_s^2}{G_sA_s^2}\right]-\frac{V_s}{A_s}\frac{dw_s}{dx}\bigg|_{x=-a}\right\}ds\\&=\frac{M_s^2}{2(EI)_s^2}\left[E_{fb}\int_{c-e_s}^{c-e_s+f_b}s^2ds+E_c\int_{-e_s-c}^{c-e_s}s^2ds\right]\\&\quad-\frac{1}{A_s}\left[\frac{\kappa_sV_s^2}{2G_sA_s}+V_s\frac{dw_s}{dx}\bigg|_{x=-a}\right]\int_{-e_s-c}^{c-e_s+f_b}ds\end{aligned} \tag{25a}$$

which results in (for plane stress assumption)

$$\begin{aligned}J_{A'F}=&\frac{M_s^2}{2(EI)_s^2}\left\{E_{fb}f_b\left[(c-e_s)(c-e_s+f_b)+\frac{f_b^2}{3}\right]\right.\\&\left.+E_c2c\left(e_s^2+\frac{c^2}{3}\right)\right\}-\frac{\kappa_sV_s^2}{2G_sb^2(2c+f_b)}-\frac{V_s}{b}w_{s,x}(-a)\end{aligned} \tag{25b}$$

Similar relations to Eq. (25) for the J-integral had been obtained for a crack in a homogeneous solid [5] or symmetric sandwich [6].

Although the elastic foundation model assumes that we have two beams connected by "distributed springs," the resulting end moment and shear on the debonded and substrate beams, calculated from the second and third derivatives of the displacement field (4a), (4b), and (4f), would involve terms of $\cosh\lambda l$ and $\sinh\lambda l$; such terms would become very large and fail the numerical calculation. Alternatively, we can assume at $x=l$ a single beam (the actual structure), which is under the moment $M_b$ and shear $V_b$. This "base" beam will have its neutral axis at a distance $e_b$ from the mid-core line (Fig. 1(a)), which is given by

$$e_b\left[E_{ft}f_t+E_c(2c)+E_{fb}f_b\right]=E_{fb}f_b\left(\frac{f_b}{2}+c\right)-E_{ft}f_t\left(\frac{f_t}{2}+c\right) \tag{26a}$$

and its flexural rigidity will be

$$\begin{aligned}(EI)_b=b\left[E_{ft}\frac{f_t^3}{12}+E_{ft}f_t\left(\frac{f_t}{2}+c+e_b\right)^2+E_c\frac{2c^3}{3}+E_c(2c)e_b^2\right.\\\left.+E_{fb}\frac{f_b^3}{12}+E_{fb}f_b\left(\frac{f_b}{2}+c-e_b\right)^2\right]\end{aligned} \tag{26b}$$

The shear modulus for the "original" sandwich beam is again derived following Ref. [15]

$$\frac{f_t+2c+f_b}{G_b}=\frac{f_t}{G_{ft}}+\frac{2c}{G_c}+\frac{f_b}{G_{fb}} \tag{26c}$$

Regarding the shear correction factor for the "base part," this is again taken from the Huang and Kardomateas [16] formula for a general asymmetric sandwich section. If we set

$$a_t=e_b+c+f_t;\quad b_t=e_b+c;\quad c_t=e_b+c+\frac{f_t}{2} \tag{26d}$$

$$a_b=-e_b+c+f_b;\quad b_b=-e_b+c;\quad c_b=-e_b+c+\frac{f_b}{2} \tag{26e}$$

and

$$d_i=\frac{E_{fi}^2}{E_c}f_i^2c_i^2+E_{fi}f_ic_ib_i^2+\frac{E_c}{4}b_i^4 \tag{26f}$$

then, the shear correction formula for the base part is given from

$$\kappa_b=\frac{b^2(f_b+2c+f_t)G_b}{(EI)_{eq}^2}\left(a_f+a_c\right) \tag{26g}$$

where

$$a_f=\sum_{i=t,b}\frac{E_{fi}^2}{4G_i}\left[a_i^4f_i-\frac{2}{3}a_i^2\left(a_i^3-b_i^3\right)+\frac{1}{5}\left(a_i^5-b_i^5\right)\right] \tag{26h}$$

$$a_c=\frac{E_c}{G_c}\sum_{i=t,b}\left[\frac{E_c}{20}\left(b_i^5-e_b^5\right)-\left(E_c\frac{b_i^2}{2}+E_{fi}f_ic_i\right)\frac{1}{3}\left(b_i^3-e_b^3\right)+d_ic\right] \tag{26i}$$

Then, the corresponding contributions to the J-integral are similar to the ones in (24) but with $M_b$ and $V_b$ in place of $M_d$ and $V_d$, respectively, and the slope at $x=l$ instead of the one at $x=-a$.

Moreover, on $EC$, $dz=ds$ and $\tau_{xz}=-V_b/A$, so in keeping with the path (Fig. 2), we obtain

$$dJ=\left[\frac{1}{2}\left(-\sigma_{xx}\epsilon_{xx}+\tau_{xz}\gamma_{xz}\right)-\tau_{xz}w_{,x}\right]ds \tag{27a}$$

For plane stress, it becomes

$$\begin{aligned}J_{EC}&=\int_{CE}\left[-E_i\frac{M_b^2s^2}{2(EI)_b^2}+\frac{\kappa_bV_b^2}{2G_bA_b^2}+\frac{V_b}{A_b}\frac{dw_b}{dx}\bigg|_{x=l}\right]ds\\&=-\frac{M_b^2}{2(EI)_b^2}\left[E_{fb}\int_{e_b-c-f_b}^{e_b-c}s^2ds+E_c\int_{e_b-c}^{e_b+c}s^2ds\right.\\&\quad\left.+E_{ft}\int_{e_b+c}^{e_b+c+f_t}s^2ds\right]+\frac{1}{A_b}\left(\frac{\kappa_bV_b^2}{2G_bA_b}+V_b\frac{dw_b}{dx}\bigg|_{x=l}\right)\int_{e_b-c-f_b}^{e_b+c+f_t}ds\end{aligned} \tag{27b}$$

which results in

$$\begin{aligned}J_{EC}=&-\frac{M_b^2}{2(EI)_b^2}\left\{E_{fb}f_b\left[(e_b-c)(e_b-c-f_b)+\frac{f_b^2}{3}\right]\right.\\&+E_c2c\left(e_b^2+\frac{c^2}{3}\right)+E_{ft}f_t\left[(e_b+c)(e_b+c+f_t)+\frac{f_t^2}{3}\right]\Big\}\\&+\frac{\kappa_bV_b^2}{2G_bb^2(f_t+2c+f_b)}+\frac{V_b}{b}w_{b,x}(l)\end{aligned} \tag{27c}$$

The displacement terms are

$$\begin{aligned}w_{d,x}(-a)&=3A_da^2-2B_da+C_d;\\w_{d,x}(l)&=\beta H_{,x}(l)+3C_5l^2+2C_6l\end{aligned} \tag{28a}$$

$$\begin{aligned}w_{s,x}(-a)&=3A_sa^2-2B_sa+C_s;\\w_{s,x}(l)&=H_{,x}(l)+3C_5l^2+2C_6l\end{aligned} \tag{28b}$$

Using (19*b*), (19*c*), and (19*d*) results in

$$w_{d,x}(-a) = -\frac{a[M_d + V_d(a/2)]}{(EI)_d} + \beta\lambda(C_2 + C_3) \tag{28c}$$

$$w_{s,x}(-a) = -\frac{a[M_s + V_s(a/2)]}{(EI)_s} + \lambda(C_2 + C_3) \tag{28d}$$

Notice that

$$w_{b,x}(l) = w_{d,x}(l) = w_{s,x}(l) \tag{28e}$$

and from (16*f*), $H_{,x}(l) = 0$, and using (11) and (12*d*)

$$w_{b,x}(l) = 3C_5 l^2 + 2C_6 l + C_7 \tag{28f}$$

Since a clamped end condition was imposed at $x = l$, it can be proved by using (11), (12*d*), and (20*c*) that $w_{b,x}(l) = 0$.

Finally, a closed form expression is obtained for the J-integral, $J = J_{BA} + J_{A'F} + J_{EC}$, by the use of (24), (27*c*), and (28*a*)–(28*f*) as

$$\begin{aligned} J = {} & \frac{6M_d^2}{E_{fl}b^2f_t^3} + \frac{M_s^2 a_s}{2(EI)_s^2} - \frac{M_b^2 a_b}{2(EI)_b^2} - \frac{\kappa_d V_d^2}{2G_d b^2 f_t} - \frac{\kappa_s V_s^2}{2G_s b^2(2c + f_b)} \\ & + \frac{\kappa_b V_b^2}{2G_b b^2(f_t + 2c + f_b)} + \frac{M_d V_d a}{b(EI)_d} + \frac{M_s V_s a}{b(EI)_s} + \frac{M_b V_b l}{b[(EI)_d + (EI)_s]} \\ & + \left[\frac{V_d^2}{(EI)_d} + \frac{V_s^2}{(EI)_s}\right]\frac{a^2}{2b} - \frac{V_b^2 l^2}{2b[(EI)_d + (EI)_s]} \\ & - \frac{\lambda}{b}(C_2 + C_3)(\beta V_d + V_s) + \frac{V_b}{b}C_7 \end{aligned} \tag{29a}$$

where

$$a_s = E_{fb}f_b\left[(c - e_s)(c - e_s + f_b) + \frac{f_b^2}{3}\right] + E_c 2c\left(e_s^2 + \frac{c^2}{3}\right) \tag{29b}$$

and

$$\begin{aligned} a_b = {} & E_{fb}f_b\left[(e_b - c)(e_b - c - f_b) + \frac{f_b^2}{3}\right] + E_c 2c\left(e_b^2 + \frac{c^2}{3}\right) \\ & + E_{ft}f_t\left[(e_b + c)(e_b + c + f_t) + \frac{f_t^2}{3}\right] \end{aligned} \tag{29c}$$

and $C_2$ and $C_3$ are given in (18*b*) and (18*c*); moreover, $C_7$ depends on the end conditions and is given in (20*c*) for the case of a clamped end. Notice that the structure of Eq. (29*a*) is similar to the one in Ref. [6]; however, Eq. (29*a*) gives the energy release rate in a fully closed form manner.

Also, notice that in the J-integral approach presented, the shear is introduced through a shear correction factor although the Euler–Bernoulli theory does not include shear. Solving for the displacement in beam problems with the Euler–Bernoulli theory, which gives simple closed form expressions, and subsequently accounting for shear using a shear correction factor, is routinely used in structural mechanics (see, for example, Ref. [14]). Since any beam theory is an approximation of the 3D elasticity, it is expected that this would present limitations. Nonetheless, the numerical results which will be presented subsequently justify the adequacy of this simple approach.

## Mode Partitioning

The complex stress intensity factor approach was used by Suo and Hutchinson [3] and Kardomateas et al. [1] to obtain the mode mixity. But the approach followed in these papers, where the complex stress intensity factor is expressed in terms of a single load-independent parameter (the $\omega$ parameter, which is determined numerically), cannot be applied here [18]. It is possible, though, to express the complex stress intensity factor in terms of several parameters (to be determined numerically) through a superposition scheme [4–6].

We emphasize again that our goal in this paper is to provide a closed form solution. Thus, an alternative approach for determining the mode partitioning is pursued, which makes use of the displacements. A new measure of mode partitioning will be introduced herein, which is based on the physical meaning of the springs in the elastic foundation approach. Notice that displacements as an alternative approach to determine mode mixity have been used in bimaterial fracture mechanics by Berggreen et al. [19]. However, the latter is based on the fracture mechanics singular field and thus it is conceptually different than our measure of mode partitioning, which is based on the elastic foundation model.

According to the Euler–Bernoulli beam theory, the displacements of the debonded part (notice that the positive slope is the counterclockwise) in the limit are

$$w_{d0} = \lim_{x\to 0} w_d(x) = D_d = \beta H(0) = \beta C_1 \tag{30a}$$

$$u_{d0} = \frac{f_t}{2}\lim_{x\to 0} w_{d,x}(x) = \frac{f_t}{2}C_d = \frac{f_t}{2}\beta H_{,x}(0) = \frac{f_t}{2}\beta\lambda(C_2 + C_3) \tag{30b}$$

and the corresponding ones for the substrate part in the limit are

$$w_{s0} = \lim_{x\to 0} w_s(x) = D_s = H(0) = C_1 \tag{30c}$$

$$\begin{aligned} u_{s0} &= -(e_s + c)\lim_{x\to 0} w_{s,x}(x) = -(e_s + c)C_s = -(e_s + c)H_{,x}(0) \\ &= -(e_s + c)\lambda(C_2 + C_3) \end{aligned} \tag{30d}$$

We can also account for the effect of transverse shear in an approximate way by including the shear strain $\gamma = \kappa V/(G_{eq}A)$ in the slope. Notice that according to Fig. 1(*a*), a positive shear would create a clockwise slope. Thus, the axial displacements at the face/core interface due to the shear, to be added to the $u_{d0}$ and $u_{s0}$, respectively, are

$$u_{d\gamma} = -\frac{f_t}{2}\frac{\kappa_d V_d}{(G_d b f_t)}; \quad u_{s\gamma} = (e_s + c)\frac{\kappa_s V_s}{[G_s b(2c + f_b)]} \tag{30e}$$

A mode partitioning phase angle, $\psi_{EF}$, based on the elastic foundation approach, may now be defined from the relative crack flank opening and shearing displacements, $\delta_w$ and $\delta_u$, respectively, at the tip; it is defined so that $\psi_{EF} = 0$ if only transverse (opening) displacement occurs at the beginning of the springs, $x = 0$ (pure mode I) and $\psi_{EF} = 90^0$ if only axial (shearing) displacement occurs at $x = 0$ (pure mode II)

$$\psi_{EF} = \tan^{-1}\left(\frac{\delta_u}{\delta_w}\right) = \tan^{-1}\frac{(u_{d0} + u_{d\gamma}) - (u_{s0} + u_{s\gamma})}{w_{d0} - w_{s0}} \tag{31a}$$

or

$$\psi_{EF} = \tan^{-1}\frac{[\beta f_t + 2(e_s + c)]\lambda(C_2 + C_3) - ((2(e_s + c)\kappa_s V_s)/(G_s b(2c + f_b))) - (\kappa_d V_d/G_d b)}{2(\beta - 1)C_1} \tag{31b}$$

It should be noted that in the elastic foundation model, a crack does not exist, instead we have beams connected by elastic springs. Therefore, this mode partitioning is not the same as the mode mixity in a bimaterial crack, which is based on the stress intensity factors from a fracture mechanics approach. As already mentioned, an alternative definition of the mode mixity based on displacements can also be defined in fracture mechanics [19] and it is also based on the ratio of the axial versus tranverse displacements near the tip of the crack.

## Rate of Energy Release by the Springs

It is also very interesting to determine the energy released by the springs when the crack grows and compare with the energy release rate, as determined by the *J*-integral. Since a crack growth by *da* means, in the context of the elastic foundation model, the "breaking" of a differential spring length *da*, we can determine the energy stored in this differential spring element, which would be released by the differential crack propagation *da*. This is $k_n\,[w_d(0) - w_s(0)]^2\,da/2$, thus the corresponding rate of energy release by the normal springs is

$$G_{SI} = \frac{1}{2}k_n[w_d(0) - w_s(0)]^2 = \frac{1}{2}k_n(\beta - 1)^2 C_1^2 \tag{32a}$$

Between the face and the core, in addition to the normal springs, there are shear spring with the following simple relation providing a very good estimate of the shear spring stiffnesses [12]

$$k_{sh} = b\frac{G_s}{c} \tag{32b}$$

Therefore, a differential shear spring length *da* would store energy $k_{sh}\,[(u_{d0} + u_{d\gamma}) - (u_{s0} + u_{s\gamma})]^2\,da/2$, thus the corresponding rate of energy release by the shear springs is

$$\begin{aligned} G_{SII} &= \frac{1}{2}k_{sh}\left[(u_{d0} + u_{d\gamma}) - (u_{s0} + u_{s\gamma})\right]^2 \\ &= \frac{1}{2}k_{sh}\left\{\left[(e_s + c) + \beta\frac{f_t}{2}\right]\lambda(C_2 + C_3) - \frac{(e_s + c)\kappa_s V_s}{G_s b(2c + f_b)} - \frac{\kappa_d V_d}{2G_d b}\right\}^2 \end{aligned} \tag{32c}$$

Accordingly, we can define another measure of mode partitioning, based on the energies released by the springs, $\psi_{SG}$, as

$$\psi_{SG} = \tan^{-1}\sqrt{\frac{G_{SII}}{G_{SI}}} = \tan^{-1}\sqrt{\frac{G_s}{c_{33}^c}}\frac{[2(e_s + c) + \beta f_t]\lambda(C_2 + C_3) - ((2(e_s + c)\kappa_s V_s)/(G_s b(2c + f_b))) - (\kappa_d V_d/G_d b)}{2(\beta - 1)C_1} \tag{32d}$$

## Results and Discussion

Results are produced for a symmetric sandwich configuration with faces made of isotropic aluminum with Young's modulus $E_f = 70$ GPa and Poisson's ratio $\nu_f = 0.3$. The core material is isotropic aluminum foam with Young's modulus $E_c = 7$ GPa and Poisson's ratio $\nu_c = 0.32$. We chose isotropic faces and core because we shall compare our results with the commercial finite element code ABAQUS, and this code can only calculate the stress intensity factors, $K_{I,II}$, for an interfacial crack when the two materials are both isotropic and linearly elastic.

In all cases, the faces had a thickness of $f_t = f_b = 2$ mm and the core had a thickness of $2c = 20$ mm. The total length of the beam was $L = 500$ mm. A debond of length $a = 200$ existed between the top face and the core.

For comparison purpose, results from the ABAQUS FEA were produced using isoparametric eight-node biquadratic plane stress elements (CPS8R) to model the sandwich beam. The singular elements were used near the crack tip to include the stress singularity (Fig. 3).

ABAQUS [20] offers the evaluation of the J-integral and stress intensity factors via its contour integral evaluation. It uses the interaction integral method [21] to calculate the stress intensity factors $K_I$ and $K_{II}$. The mode mixity from the FEA analysis is further calculated from

$$\psi_{\text{FEA}} = \tan^{-1}\left(\frac{K_{II}}{K_I}\right) \tag{33}$$

It should be noticed that although ABAQUS has the option to calculate the energy release rates of modes I and II, $G_I$ and $G_{II}$, respectively, through the virtual crack closure technique, the values were widely varying depending on the mesh size at the crack tip. Same oscillation of values has been observed at other studies of interfacial cracks [22]. Thus, the energy release rate components, $G_I$ and $G_{II}$, cannot be used directly to estimate a related energy-release-rate-based mode mixity from ABAQUS.

Table 1 shows the energy release rate values from the closed form expression (29) from the present elastic foundation analysis, $J_{\text{EF}}$ in comparison with the one computed from the finite element analysis, and $J_{\text{FEA}}$ for a range of loading combinations. We have used the subscript EF to denote results from our elastic foundation approach and FEA to denote results from the finite element code ABAQUS. It can be seen that there is a very good agreement. In addition, Table 1 shows the values of the normal spring energy release rate, $G_{SI}$, and the sum of the normal and shear spring energy release rate, $G_{SI} + G_{SII}$. It can be seen that the $G_{SI}$ is very close to the J-integral in all cases except when the substrate is heavily loaded (fifth and seventh cases in Table 1), in which cases the shear spring energy release rate is needed to approach the J-integral values. In particular, case 7 in which the only load is a shear force applied to the substrate (which includes the weak core) shows that the energy released by the shear springs is significant in this case. In case 5, in which a large shear is applied to the substrate (in addition to loading the debonded part), the $J_{\text{FEA}}$ is noticeably larger than the $J_{\text{EF}}$, and this can also be attributed to the significant shear loading of the core, which can be accounted for by the energy released by the shear springs. Notice that our elastic foundation analysis uses a simple shear correction angle to account for the shear contribution of the core but this is expected to be inadequate in cases of large shear loading of the core (high-order shear analyses could be needed in such cases as has been demonstrated in Ref. [13]).

**Table 1 Energy release rates**

| $V_d$ (N) | $V_s$ (N) | $M_d$ (N mm) | $M_s$ (N mm) | $J_{\text{EF}}$ (N/mm) | $G_{SI}$ (N/mm) | $(G_{SI} + G_{SII})$ (N/mm) | $J_{\text{FEA}}$ (N/mm) |
|---|---|---|---|---|---|---|---|
| 0.5 | −0.5 | 100 | −100 | 0.4381 | 0.4381 | 0.4701 | 0.4356 |
| 1.0 | −1.0 | 50 | −50 | 0.6920 | 0.6920 | 0.7417 | 0.6859 |
| 1.0 | −1.0 | 100 | 100 | 0.9880 | 0.9871 | 1.058 | 0.9804 |
| 10.0 | −1.0 | 100 | −100 | 48.66 | 48.80 | 52.40 | 48.33 |
| 1.0 | −10.0 | 100 | −100 | 0.8944 | 1.034 | 1.093 | 1.1165 |
| 0.5 | 0.0 | 0 | 0 | 0.1103 | 0.1107 | 0.1189 | 0.1097 |
| 0.0 | −0.5 | 0 | 0 | $3.0 \times 10^{-4}$ | $1.4 \times 10^{-4}$ | $3.5 \times 10^{-4}$ | $2.7 \times 10^{-4}$ |
| 0.0 | 0.0 | 100 | 0 | 0.1070 | 0.1068 | 0.1148 | 0.1070 |

**Table 2 Mode partitioning measures**

| $V_d$ (N) | $V_s$ (N) | $M_d$ (N mm) | $M_s$ (N mm) | $\psi_{SG}$ (deg) | $\psi_{EF}$ (deg) | $\psi_{FEA}$ (deg) |
|---|---|---|---|---|---|---|
| 0.5 | −0.5 | 100 | −100 | 15.1 | −26.7 | −28.5 |
| 1.0 | −1.0 | 50 | −50 | 15.0 | −26.5 | −28.4 |
| 1.0 | −1.0 | 100 | 100 | 15.1 | −26.6 | −30.3 |
| 10.0 | −1.0 | 100 | −100 | 15.2 | −26.8 | −30.8 |
| 1.0 | −10.0 | 100 | −100 | 13.4 | −23.8 | −12.5 |
| 0.5 | 0.0 | 0 | 0 | 15.2 | −26.9 | −31.2 |
| 0.0 | −0.5 | 0 | 0 | 51.1 | 66.5 | 56.9 |
| 0.0 | 0.0 | 100 | 0 | 15.3 | −27.0 | −31.5 |

Table 2 shows the mode partitioning measures for the same combination of loads as in Table 1. The mode partitioning measure defined in the context of the elastic foundation analysis, $\psi_{EF}$, is in good agreement with the mode mixity from the finite element analysis, $\psi_{FEA}$, the different physical concepts that are each based on notwithstanding (the $\psi_{EF}$ is based on the displacements at the "debond tip spring" and the $\psi_{FEA}$ on the stress intensity factors at the interface crack). The mode partitioning measure based on the energy released by the differential spring at the "debond tip," $\psi_{SG}$, is always positive and different than the other values, as expected, but it trends the same way, i.e., it shows the relatively small amount of mode II in all cases except the one where the shear load is applied exclusively to the substrate (second case from the end of the tables) where a large amount of shear is present due to the loading of the core. In that case, all measures capture this large amount of shear.

Although the focus of this paper is to present the concepts (elastic foundation approach, mode partitioning definitions, etc.) and the mathematics (detailed closed form expressions), rather than an extensive parametric study on the geometry and materials (which will be the topic of a subsequent report), we produced data for the case of a much smaller crack, namely, for a crack length of $a = 20$ mm (as opposed to $a = 200$ mm in Tables 1 and 2) and for the case 2 of the tables, i.e., $V_d = -V_s = 1.0$ Nt and $M_d = -M_s = 50$ N mm. The elastic foundation approach resulted in $J_{EF} = 0.0584$ Nt/mm whereas ABAQUS resulted in $J_{FEA} = 0.0567$ Nt/mm. Regarding mode partitioning, the elastic foundation approach resulted in $\psi_{EF} = -25.3$ deg and ABAQUS in $\psi_{FEA} = -27.8$ deg. The elastic foundation approach captures the trend for a slightly lower mode partitioning measure of the smaller crack by about one degree and the agreement with the J-integral is also very good and slightly larger value in the elastic foundation approach for both crack lengths. Thus, it can be concluded that the accuracy of the elastic foundation model is not compromised when the crack lengths are smaller. However, similar to the statement made in Ref. [6], the presented elastic foundation approach is not expected to be applicable for very small debond lengths, i.e., when the debond length is so small that the crack tip singular stresses interact with the edges.

It should again be emphasized that in the elastic foundation approach, there is no crack as defined by the conventional fracture mechanics, i.e., there is no crack tip beyond which the top face and the core are bonded and have the same axial and transverse displacements. On the contrary, normal and shear springs are considered at the interface, thus there is a gap between the top face and the core in the mathematical elastic foundation model. Therefore, we cannot define the mode-mixity based on stress intensity factors and singular stress fields, as is done in conventional fracture mechanics. Instead, we have proposed a new measure for the relative amounts of modes I and II, which we call mode partitioning, and which is the ratio of the transverse displacement to the axial displacement of springs at the tip (point where the springs start). It is interesting to notice that this newly proposed mode partitioning can provide a good estimate of the mode mixity, as is done in fracture mechanics. Meanwhile, differences are observed in some cases and it is natural to expect that there will be cases of material combinations and/or loadings for which this simplified model may not be as accurate. In particular, case 5 in Table 2, in which the substrate (which includes the core) is loaded by a large shear force, shows a noticeable difference between the elastic foundation and the finite element analysis results. This is expected since our elastic foundation analysis uses a simple shear correction angle to account for the shear contribution of the core, but this is expected to be inadequate in cases of large shear loading of the core. A Timoshenko-based, first-order shear analysis or high-order shear theory could lead to better accuracy. More studies on the mode partitioning measure from the present paper and the stress-intensity-factor-based mode mixity from fracture mechanics, including a parametric study, will be carried out and reported in a separate paper.

## Conclusions

Closed form expressions for the energy release rate and mode partitioning of face/core debonds in shear loaded sandwich composites are derived. An elastic foundation approach is pursued along with the Euler–Bernoulli theory for the four different parts of the structure (free and joined debonded and substrate parts) with a simple shear correction angle added. Unlike other studies in the literature, this analysis is comprehensive and includes the deformation of the substrate part, which consists of both the core and the bottom face, and, furthermore, the analysis is done for a general asymmetric sandwich construction. The J-integral is used to derive a closed form expression for the energy release rate. It is shown that the energy release rate is very close to the differential energy stored in the springs at the beginning of the elastic foundation, i.e., the energy released by the "broken" differential spring element as the debond propagates. In addition, the J-integral shows excellent agreement with the corresponding values from a finite element analysis where the debond is considered an interface crack. The transverse and axial displacements at the beginning of the elastic foundation ("debond tip") are used to define a mode partitioning measure in the context of this elastic foundation approach. A comparison with finite element results shows that this mode partitioning measure values are close to the traditional mode mixity values of the corresponding interfacial cracks.

## Acknowledgment

The financial support of the Federal Aviation Administration (Funder ID: 10.13039/100006282) though the National Aerospace Institute Cooperative Agreement 16-P-0012 is acknowledged. The interest and encouragement of the Grant Monitors Dr. Zhi-Ming Chen, Dr. Ronald Krueger, Dr. Larry Ilcewicz, Dr. Peter McHugh, and Dr. Curtis Davies, and that of the Office of Naval Research (Grant Nos. N00014-16-1-2831 and N00014-16-1-2448; Funder ID: 10.13039/10000000), and the interest and encouragement of the Grant Monitor, Dr. Y.D.S. Rajapakse, are gratefully acknowledged. The research in this paper is part of the Masters of Science thesis of the second author (Niels Pichler) at the Ecole Polytechnique Federale de Lausanne.

## References

[1] Kardomateas, G. A., Berggreen, C., and Carlsson, L. A., 2013, "Energy-Release Rate and Mode Mixity of Face/Core Debonds in Sandwich Beams," AIAA J., **51**(4), pp. 885–892.
[2] Østergaard, R. C., and Sørensen, B. F., 2007, "Interface Crack in Sandwich Specimen," Int. J. Fract., **143**(4), pp. 301–316.
[3] Suo, Z., and Hutchinson, J. W., 1990, "Interface Crack Between Two Elastic Layers," Int. J. Fract., **43**(1), pp. 1–18.
[4] Li, S., Wang, J., and Thouless, M. D., 2004, "The Effects of Shear on Delamination in Layered Materials," J. Mech. Phys. Solids, **52**(1), pp. 193–214.
[5] Andrews, M. G., and Massabò, R., 2007, "The Effects of Shear and Near Tip Deformations on Energy Release Rate and Mode Mixity of Edge-Cracked Orthotropic Layers," Eng. Fract. Mech., **74**(17), pp. 2700–2720.

[6] Barbieri, L., Massabò, R., and Berggreen, C., 2018, "The Effects of Shear and Near Tip Deformations on Interface Fracture of Symmetric Sandwich Beams," Eng. Fract. Mech., **201**, pp. 298–321.
[7] Kanninen, M. F., 1973, "An Augmented Double Cantilever Beam Model for Studying Crack Propagation and Arrest," Int. J. Fract., **9**(1), pp. 83–92.
[8] Williams, J. G., 1989, "End Corrections for Orthotropic DCB Specimens," Compos. Sci. Technol., **35**(4), pp. 367–376.
[9] Thouless, M. D., 2018, "Shear Forces, Root Rotations, Phase Angles and Delamination of Layered Materials," Eng. Fract. Mech., **191**, pp. 153–167.
[10] Li, X., and Carlsson, L. A., 2000, "Elastic Foundation Analysis of Tilted Sandwich Debond (TSD) Specimen," J. Sandwich Struct. Mater., **2**(1), pp. 3–32.
[11] Saseendran, V., Carlsson, L. A., and Berggreen, C., 2018, "Shear and Foundation Effects on Crack Root Rotation and Mode-Mixity in Moment- and Force-Loaded Single Cantilever Beam Sandwich Specimen," J. Compos. Mater., **52**(18), pp. 2537–2547.
[12] Kardomateas, G. A., Yuan, Z., and Carlsson, L. A., 2018, "Elastic Foundation Constants for Sandwich Composites," AIAA J., **56**(10), pp. 4169–4179.
[13] Phan, C. N., Frostig, Y., and Kardomateas, G. A., 2012, "Analysis of Sandwich Beams With a Compliant Core and With In-Plane Rigidity–Extended High-Order Sandwich Panel Theory Versus Elasticity," ASME J. Appl. Mech., **79**(4), pp. 041001-1–041001-11.
[14] Timoshenko, S., and Gere, J. M., 1966, *Theory of Elastic Stability*, McGraw-Hill, New York.
[15] Kardomateas, G. A., and Simitses, G. J., 2004, "Buckling of Long Sandwich Cylindrical Shells Under External Pressure," ASME J. Appl. Mech., **72**(4), pp. 493–499.
[16] Huang, H., and Kardomateas, G. A., 2002, "Buckling and Initial Postbuckling Behavior of Sandwich Beams Including Transverse Shear," AIAA J., **40**(11), pp. 2331–2335.
[17] Carlsson, L., and Kardomateas, G., 2011, *Structural and Failure Mechanics of Sandwich Composites*, Springer, New York.
[18] Pichler, N., 2018, "Energy Release Rate and Mode Mixity of Face/Core Debonds in Sandwich Composites," Master's thesis, Gnie Mcanique, Ecole Polytechnique Fédérale de Lausanne, Lausanne, February.
[19] Berggreen, C., Simonsen, B. C., and Borum, K. K., 2007, "Experimental and Numerical Study of Interface Crack Propagation in Foam-Cored Sandwich Beams," J. Compos. Mater., **41**(4), pp. 493–520.
[20] Dassault Systems Simulia Corp., 2018, *SIMULIA User Assistance 2018*, Dassault Systems Simulia Corp, Providence, RI.
[21] Shih, C. F., and Asaro, R. J., 1988, "Elastic-Plastic Analysis of Cracks on Bimaterial Interfaces: Part I—Small Scale Yielding," ASME J. Appl. Mech., **55**(2), pp. 299–316.
[22] Raju, I. S., Crews, J. H., and Aminpour, M. A., 1988, "Convergence of Strain Energy Release Rate Components for Edge-Delaminated Composite Laminates," Eng. Fract. Mech., **30**(3), pp. 383–396.